PFG 2012 / 3, 0267–0280
Stuttgart, June 2012

Article

A Decision Fusion Framework for Hyperspectral Subpixel Target Detection

Hamed Gholizadeh, Mohammad Javad Valadan Zoej & Barat Mojaradi, Tehran, Iran

Keywords: Target detection, decision fusion, hyperspectral data, remote sensing

Summary: Target detection is one of the most challenging issues of remotely sensed data. Due to high spectral resolution of the hyperspectral images and their limited ground sampling distance, targets of interest occur at subpixel level. In such cases, spatial characteristics of targets are hard to acquire and the only way to overcome such problem is to take advantage of the spectral information. Based on the spectral characteristics of background and the targets to be detected, several methods have been proposed. Some of these methods assume a physics-based approach, while the other may be purely statistical. So, all of these methods are based on some assumptions each of which can be challenged in one way or another. One possible way to take advantage of these differences to improve the final results is the fusion of the detectors' outputs. In this paper, eight subpixel target detectors are employed as the ensemble detectors. It is also worth mentioning that the detectors should be different from each other; otherwise the overall decision will not be better than the individual detectors. So, we suggest using the genetic algorithms to select the most suitable detectors for a given decision fusion rule. Experimental results on a real world hyperspectral data as well as a synthetic dataset show the efficiency of the proposed method to improve the detection performance.

Zusammenfassung: *Die Objekterkennung in Fernerkundungsszenen ist bislang nur teilweise gelöst.* Im Fall von Hyperspektraldaten steht der hohen spektralen eine begrenzte räumliche Auflösung gegenüber. Daher sind viele Objekte kleiner als ein Pixel, so dass eine Aussage über die geometrischen Eigenschaften nur eingeschränkt möglich ist. Daher kommt der spektralen Information eine erhöhte Bedeutung zu. In der Vergangenheit wurden viele Analysemethoden vorgeschlagen, die die Objekterkennung nach den spektralen Charakteristiken der gesuchten Objekte und ihrer Umgebung, dem Bildhintergrund, erlauben, Einige der Methoden verfolgen modellbasierte Ansätze während andere rein statistisch arbeiten. Alle Methoden erfordern spezifische Annahmen, die eine zusätzliche Unsicherheit für das Ergebnis bedeuten. Ein Ansatz zur Verbesserung des Gesamtergebnisses ist die Verschneidung (Fusion) der mit den unterschiedlichen Methoden (Detektoren) gefundenen Einzelergebnisse.

In diesem Artikel werden acht typische Detektoren beispielhaft untersucht und gezeigt, wie mit Hilfe der Methode Genetischer Algorithmus die für eine gegebene Fragestellung geeignetste Kombination gefunden werden kann. Die Methode wird sowohl an echten als auch an synthetischen Hyperspektraldaten erprobt. Die Untersuchung zeigt, dass die vorgeschlagene Methode die Erkennbarkeit von Objekten verbessert.

1 Introduction

Spectral subpixel detection in hyperspectral image (HSI) data aims to identify a target smaller than the size of a pixel using only spectral information (Broadwater & Chellappa 2007). This *a priori* information may be obtained from *in situ* measurements, a spectral library or can be image derived.

Subpixel target detectors are completely dependent on how the scene endmembers are modeled. If the total surface area is conceived to be divided proportionally according to the fractional abundances of the constituent subspaces, then there exists a linear relation between the fractional abundances of the substances comprising the area being imaged, and the spectra in the reflected radiation

www.schweizerbart.de
DOI: 10.1127/1432-8364/2012/0116
1432-8364/12/0116 $ 3.50

(Manolakis et al. 2003). Hence, this is called the linear mixing model (LMM), and is expressed as

$$r = \sum_{j=1}^{p} \alpha_j m_j + n = M\alpha + n \quad (1)$$

where r is the $l \times 1$ received pixel spectrum vector, m_j which represents the j-th endmember, is the j-th $l \times 1$ column of M, α is the P × 1 fraction abundance column vector, n is the $l \times 1$ additive observation noise vector, M is the $l \times P$ matrix whose columns are m_j, l is the number of spectral bands and P is the number of endmembers.

We may confront a more complicated scenario in which the substances comprising the medium are organized proportionally on the surface. This intimate mixture results when each component is randomly distributed in a homogeneous way. As a result, the incident radiation may no longer uphold the linear properties of the constituent substance spectra. This scenario is referred to as non linear mixing (Manolakis et al. 2003).

Conventional subpixel target detectors can be divided into four categories (Broadwater & Chellappa 2007): One of the earliest methods uses array processing techniques to nullify the background signatures as one would nullify an interfering signature when performing beamforming (Broadwater & Chellappa 2007). The orthogonal subspace projection (OSP) (Harsanyi & Chang 1994), constrained energy minimization (CEM) (Chang & Heinz 2000) and target constrained interference minimized filter (TCIMF) (Ren & Chang 2000) algorithms are examples of such methods. Another approach uses the linear mixing model to directly estimate the abundance values and uses the estimated target abundances for detection purposes (Broadwater & Chellappa 2007). Fully constrained least squares (FCLS) (Heinz et al. 1999), non-negatively constrained least squares (NCLS) (Bro & Jong 1997) and sum-to-one constrained least squares (SCLS) fall within this category. Since FCLS and NCLS attempt to address the phenomenological constraints in the linear mixing model, they can be considered physics-based (Broadwater & Chellappa 2007). There are other kinds of subpixel target detectors which are based on a statistical hypothesis test. Adaptive matched subspace detector (AMSD) (Manolakis et al. 2001) is a statistical target detector based on structured background. Unlike AMSD, adaptive cosine/coherent estimate (ACE) (Kraut et al. 2005), which is another statistical target detector, assumes no structured background.

It is also well known that in many situations combining the output of several classifiers leads to an improved classification result. This happens because the subset of the input space that one classifier will attribute a correct label will differ from the other. This implies that by using information from more than one classifier it is probable that a better overall accuracy can be obtained for a given problem (Alexandre et al. 2001). A single classifier is generally unable to handle the wide variability and scalability of the data in any problem domain (Mangari et al. 2010). There are mainly three types of fusion strategies (Dasarathy 1994), namely, information/data fusion (low-level fusion), feature fusion (intermediate-level fusion), and decision fusion (high level fusion). In this paper the fusion process is carried out on decision level.

The aim of this paper is the decision fusion of 8 subpixel target detectors. Since there might be cases in which some detectors show similar performance, we employed the genetic algorithms (GA) to choose the most optimum detectors as the fusion input.

The remainder of this paper is organized as follows. Section 2 describes eight subpixel detection methods. Section 3 briefly reviews decision fusion approaches and the proposed method. Performance comparison of the proposed method is provided in section 4 and the conclusions are included in section 5.

2 Conventional Subpixel Target Detectors

2.1 *Orthogonal Subspace Projection (OSP)*

In OSP, the endmember matrix M in (1) is divided into two parts: desired signature vector ($d = m_p$) and undesired signature matrix ($U = [m_1, m_2, \ldots, m_{p-1}]$. Then, we can rewrite (1) as

$$r = d\alpha_p + U\gamma + n \tag{2}$$

where α_p is the abundance fraction of the desired signature and γ is a $(p-1) \times 1$ abundance fraction vector of the undesired signatures. To suppress the undesired target, the orthogonal projection operator ($P_U^{\perp}$), which maps data onto a subspace orthogonal to the undesired signatures space, is used.

$$P_U^{\perp} = I - U(U^T U)^{-1} U^T \tag{3}$$

where I denotes the $L \times L$ identity matrix.

Applying $P_U^{\perp}$, under the white-noise assumption (Du et al. 2003), results in the OSP detector

$$\delta_{OSP} = d \;\; P_U^{\perp} r \tag{4}$$

2.2 *Constrained Energy Minimization (CEM)*

In order to implement OSP, knowledge of all target signatures of interest is required. Such knowledge is generally difficult to obtain in practice (Chang & Heinz 2000). So, CEM is developed for the case that the only available knowledge is the signature to be classified. The CEM algorithm tries to maximize the response of the target spectral signature while minimizing the response of the unknown background signatures. The algorithm uses an estimate of the sample correlation matrix as a basis for determining the unknown background signatures and is computationally efficient. It also does not assume the linear mixture model or any noise characteristics (Du et al. 2003).

The CEM detector can be given by

$$\delta_{CEM}(r) = (d^T R_{L\times L}^{-1} d)^{-1} (R_{L\times L}^{-1} d)^T r \tag{5}$$

where R is the sample correlation matrix.

The CEM generally outperforms the OSP in terms of eliminating unidentified signal source and suppressing noise, but it has a poor generalization property since it is very sensitive to the knowledge used for the desired target as well as the noise (Chang & Heinz 2000).

2.3 *Target Constrained Interference Minimized Filter (TCIMF)*

Compared to the OSP that only deals with desired and undesired signal sources and the CEM that only considers the desired signal source without taking into account the undesired ones, the TCIMF combines both the OSP and the CEM into one filter operation. Interestingly, the CEM and the TCIMF can be also interpreted as various versions of the OSP operating different degrees of target knowledge (Chang 2005).

Consider $D = [d_1, d_2, \ldots, d_p]$ as the desired target signatures and $U = [u_1, u_2, \ldots, u_q]$ be the undesired target signature matrix, the TCIMF detector can be stated as

$$\delta_{TCIMF}(r) = (w^{TCIMF})^T r \tag{6}$$

where

$$w_{TCIMF} = R_{L\times L}^{-1}[DU]([DU]^T R_{L\times L}^{-1}[DU])^{-1} \begin{bmatrix} 1_{p\times 1} \\ 0_{q\times 1} \end{bmatrix} \tag{7}$$

2.4 *Fully Constrained Least Squares (FCLS)*

To make the LMM have physical meaning, two constraints are defined: the abundance nonnegative constraint (ANC) and the abundance sum-to-one constraint (ASC) (Zhang et al. 2010).

$$\sum_{j=1}^{p} \alpha_j = 1 \tag{8}$$

$$\alpha_j \geq 0 \qquad for \qquad 1 \leq j \leq p \tag{9}$$

With these two criteria, exact abundance fractions would be extracted.

What makes the FCLS algorithm different from the previously mentioned algorithms, is that both the nonnegativity and sum-to-one constraints are handled simultaneously (Heinz & Chang 2001). Therefore, the FCLS solution provides abundance estimates that meet the linear mixing model constraints, but does not allow a closed-form mathematical solution due to the non-negativity constraints. Instead, a numerical solution is proposed (Broadwater

& Chellappa 2007). In FCLS, the endmember matrix (M) and pixel signatures (r) are extended such that:

$$N = \begin{bmatrix} \sigma M \\ 1^T \end{bmatrix} \tag{10}$$

$$S = \begin{bmatrix} \sigma r \\ 1 \end{bmatrix} \tag{11}$$

where $1 = [1, 1, \ldots, 1]^T$ is a $p \times 1$ vector. The parameter σ is a small number (typically 1×10^{-5}) controlling how close the resulting abundances would sum to one. After the aforementioned procedure, the next step is to minimize the least squares error (LSE) by estimating the non-negative abundance values, which can be expressed as:

$$\text{minimize LSE } \{(N\alpha\text{-}S)^T(N\alpha\text{-}S)\} \text{ subject to } \alpha \geq 0 \tag{12}$$

Using the Lagrange multipliers, the following function can be defined.

$$J = \frac{1}{2}(N\alpha - S)^T(N\alpha - S) + \lambda(\alpha - c) \tag{13}$$

where c is an unknown constant vector and each member of this vector is nonnegative to enforce the nonnegativity constraint.

$$\left(\frac{\partial J}{\partial \alpha}\right)\Big|_{\hat{\alpha}_{FCLS}} \text{ and } \alpha = c.$$

So, the obtained equation contains two unknowns: the abundance estimates and the Lagrange multipliers. Solving for these unknown results in

$$\hat{\alpha}_{FCLS} = (N^T N)^{-1} N^T S - (N^T N)^{-1}\lambda = \hat{\alpha}_{LS} - (N^T N)^{-1}\lambda \tag{14}$$

and

$$\lambda = N^T(S - N\hat{\alpha}_{FCLS}) \tag{15}$$

In (14) $\hat{\alpha}_{LS}$ is unconstrained least squares solution.

Iterating through (14) and (15) provides the numerical solution for the non-negativity constraints. To begin this iterative method, set all the Lagrange multipliers to zero and calculate the abundance using (14). Note that for first iteration unconstrained least squares solution will be used. At each iteration, those indices (Lagrange multipliers) corresponding positive abundance fractions are placed in the passive set P and the remainder abundance fractions are placed in the active set R. Iterate (14) and (15) until all Lagrange multipliers in the passive set are zero and all Lagrange multipliers in the active set are either zero or negative. At this point, the Kuhn-Tucker conditions are satisfied and an optimal mean-squared error solution for the unmixing of the image can be obtained.

2.5 *Nonnegatively Constrained Least Squares (NCLS)*

The idea of NCLS is to minimize the LSE by estimating the non-negative abundance values. In other words, to solve the following optimal problem

$$\text{minimize LSE } \{(r - M\alpha)^T(r - M\alpha)\} \text{ subject to } \alpha \geq 0 \tag{16}$$

As can be seen, the solution provided in (14) and (15) accounts for both the nonnegativity and sum-to-one constraints. So, the answer to the NCLS is straightforward. To handle the nonnegativity constraint, the modifications applied to the endmember matrix (M) and the pixel signatures (r) will be eliminated, i.e., the sum-to-one constraint will be ignored.

2.6 *Sum-to-one Constrained Least Squares (SCLS)*

Unlike FCLS and NCLS, the SCLS method produces a closed form solution. The SCLS solves the following optimization problem:

$$\text{minimize LSE}\{(\mathbf{r} - M\alpha)^T(\mathbf{r} - M\alpha)\} \text{ subject to } \Delta = \{\alpha \Big| \textstyle\sum_{j=1}^{p} \alpha_j = 1\} \tag{17}$$

The answer to this problem can be expressed as:

$$\hat{\alpha}_{SCLS}(r) = P^{\perp}_{M,l}\hat{\alpha}_{LS}(r) + (M^T M)^{-1}\mathbf{1}[\mathbf{1}^T(M^T M)^{-1}\mathbf{1}]^{-1} \tag{18}$$

where

$$P_{M,l}^{\perp} = I_{L\times L} - (M^T M)^{-1}\mathbf{l}[\mathbf{l}^T(M^T M)^{-1}\mathbf{l}]^{-1}\mathbf{l}^T \quad (19)$$

and $\mathrm{l} = [\mathrm{l}, \mathrm{l}, \ldots, \mathrm{l}]^T$ is a $p \times 1$ vector.

2.7 *Adaptive Matched Subspace Detector (AMSD)*

Another kind of subpixel target detection method is based on a statistical hypothesis test. Adaptive matched subspace detector (AMSD) is such an algorithm that formulates the target and background subspaces and uses the LMM and the generalized likelihood ratio test (GLRT) to separate a probable subpixel target (Manolakis et al. 2001). AMSD uses the LMM; however, the sum-to-one and nonnegativity constraints are not satisfied. To develop such algorithm, we establish the following hypothesis tests

$$\begin{aligned} H_0&: r = Ba_{b,0} + n = Sa_{b,0} + w, w \sim \mathrm{N}(0, \sigma_{\mathrm{w}}^2 I) \\ H_1&: r = Sa_s + Ba_{b,1} + n = Sa + w \end{aligned} \quad (20)$$

where H_0 is the null hypothesis (target absent) and H_1 is the alternate hypothesis (target present). In the AMSD, the noise is assumed as a zero mean normal distribution with covariance matrix σI. Then, the hypotheses are expressed as

$$\begin{aligned} H_0&: r \sim N(Ba_{b,0}, \sigma_0^2 I) \\ H_1&: r \sim N(Sa_s + Ba_{b,1}, \sigma_1^2 I) \end{aligned} \quad (21)$$

In practice, noise variance σ_w^2 and abundance vector a are unknown and should be estimated from image data using maximum likelihood estimation (MLE) for both the null and alternate hypotheses. Afterwards, taking the derivative of the MLEs with respect to each of the unknown parameters and setting them equal to zero, the MLE estimate of abundance and noise variance are found. After some algebraic manipulations and forming the GLRT, the AMSD detector will be obtained

$$D_{AMSD}(r) = \frac{r^T(P_B^{\perp} - P_Z^{\perp})r}{r^T P_Z^{\perp} r} \quad (22)$$

where B contains the background signatures, and Z is defined as the concatenation of the target and background signatures.

2.8 *Adaptive Cosine/Coherent Estimator (ACE)*

We may focus on modeling the background in a stochastic sense. Here, we think of finding a mean centred target in additive background noise. Therefore, the model we assume is

$$\begin{aligned} H_0&: r \sim N(0, \sigma_0^2 \Gamma) \\ H_1&: r \sim N(Sa_s, \sigma_1^2 \Gamma) \end{aligned} \quad (23)$$

where $\Gamma = \frac{1}{N}\sum_{i=1}^{N} r(i)r^T(i)$ is the MLE of the covariance matrix. N is the number of background pixels in the image. If we assume that N is very large, the covariance estimate from these likelihoods can be simplified to $\Gamma = \sum_{i=1}^{N} r(i)r^T(i)$, which is a standard assumption made in the literature. Referring to (20), the ACE algorithm sets $B = 0$, therefore the sum-to-one and nonnegativity constraints cannot be met either as they require a background subspace (Broadwater & Chellappa 2007).

The ACE detector can be expressed as

$$D_{ACE}(r) = \frac{r^T \hat{\Gamma}^{-1} S(S^T \Gamma^{-1} S) S^T \Gamma^{-1} r}{r^T \hat{\Gamma}^{-1} r} \quad (24)$$

Despite this seemingly simple background model, the ACE detector is one of the most powerful subpixel detectors available for HSI data (Manolakis & Shaw 2002).

3 Decision Fusion

As stated before, in this paper the fusion process is carried out on decision level, so this section gives an insight into the decision fusion methods. Fusion at decision level can be divided into three categories based on the type of the classifier outputs (Xu et al. 1992):

Type 1 (abstract level): given L classifiers each classifier (D_i) outputs a class label. So, for

any input object (x) to be classified, the L classifiers define a vector $s=[s_1,s_2,...,s_L]^T \in \Omega^L$ where $\Omega=\{\omega_1,\omega_2,...,\omega_c\}$ is the set of class labels. In the simplest fusion scheme, the ensemble chooses the class which receives the highest number of votes (majority voting).

Type 2 (rank level): the output of each D_i is a subset of Ω, with the alternatives ranked in order of plausibility of being correct label.

Type 3 (measurement level) each classifier outputs a c-dimensional vector of measurements $[d_{i,1},d_{i,2},\ldots,d_{i,c}]$, each value of this vector represents how likely a label is.

3.1 *Decision Fusion Approaches*

Product rule: This rule is good if the individual classifiers are independent, i.e., that the outcomes of $d_{i,j}$ for random x are independent for fixed i (classifier) and variable j (class). This is hardly ever the case.

$$\mu_j(x)=\prod_i^L d_{i,j} \qquad ,j=1,...,c \tag{25}$$

The rule assumes noise free and reliable confidence estimates. It fails if these estimates may be accidentally zero or very small (Duin 2002).

Mean rule: In case the base classifiers contain independent noise behaviour, the errors in the confidences are averaged out by the summation (Duin 2002).

$$\mu_j(x)=\frac{1}{L}\sum_{i=1}^L d_{i,j} \qquad ,j=1,...,c \tag{26}$$

Maximum rule: At first glance this seems reasonable: select the classifier that is most confident of itself. However, this assumption immediately fails, if some classifiers are more overtrained than others. In that case they may be overconfident and thereby dominating the outcome, without having a better performance (Duin 2002).

$$\mu_j(x)=\max_{i=1}^L d_{i,j} \qquad ,j=1,...,c \tag{27}$$

Minimum rule: Like for the maximum rule, a good example of a situation in which this rule is really adequate is hard to find (Duin 2002).

$$\mu_j(x)=\min_{i=1}^L d_{i,j} \qquad ,j=1,...,c \tag{28}$$

Median rule: The mean and the median methods have approximately the same performance for normally distributed data but are different for the uniform distribution, the average being the better of the two (Kuncheva 2002).

$$\mu_j(x)=med_{i=1}^L d_{i,j} \qquad ,j=1,...,c \tag{29}$$

3.2 *Proposed Fusion Scheme*

In real world hyperspectal applications especially target detection, training data are limited or it is expensive to collect such data for all phenomena. In particular, when spectra of several targets are known and ground truth of only a few are available. So, this motivated us to design a scheme which makes use of available knowledge and is capable to generalize it for other targets.

The block diagram of the proposed fusion scheme is shown in Fig. 1. The proposed framework is as follows. For the detectors which require to know the spectra of all endmembers present in the scene, the HySime (Bioucas-Dias & Nascimento 2008) coupled with the vertex component analysis (VCA) (Nascimento & Bioucas-Dias 2005) are employed to extract such knowledge. In case of using CEM and ACE, the only required knowledge is the targets' spectra. However, due to sensitivity of the CEM detector to noise (Chang & Heinz 2000), which is the function of the sample correlation matrix rank, only a subset of eigenvectors is used to calculate the inverse of sample correlation matrix. The number of eigenvectors is determined through singular value decomposition (SVD) (Chang & Heinz 2000). After generating detection results for each target, the individual decisions are aggregated through the aforementioned decision fusion rules. As shown in (Kuncheva 2002), apart from the fusion methods, diversity among classifiers can provide higher classification accuracies. In case of target detection, corresponding to each decision fusion rule, the most optimum detectors can be chosen using a search strategy. In fact, we aim at improving detection performance through choosing

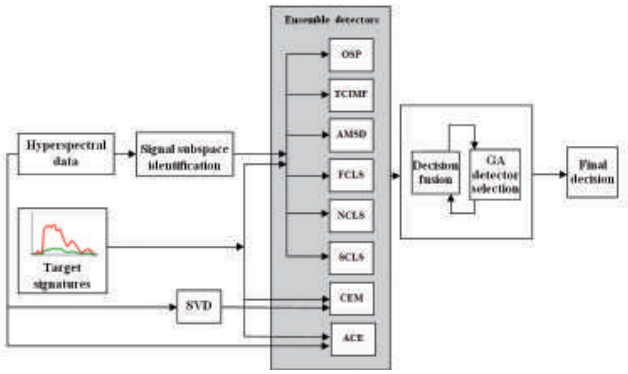

Fig. 1: Architecture of the proposed detector fusion scheme, SVD = singular value decomposition, OSP = orthogonal subspace projection, TCIMF = target constrained interference minimized filter, AMSD = adaptive matched subspace detector, FCLS = fully constrained least squares, NCLS = nonnegatively constrained least squares, SCLS = sum-to-one constrained least squares, CEM = constrained energy minimization, ACE = adaptive cosine/coherent estimator.

the most effective detectors for each decision rule. A possible way to reach this goal is to take advantage of GA. This approach may allocate distinct banks of detectors for each decision rule through GA.

4 Experimental Results and Discussion

4.1 *Dataset Description*

Synthetic dataset: To evaluate the subpixel detection performance, a synthetic image consisting of 54 × 54 mixed pixels is simulated. In order to generate the background image, three materials' spectra were selected and mixed according to a Dirichlet distribution. The spectra of both background and target pixels were obtained from Indian Pines dataset (Hsieh & Landgrebe 1998) (after removing noisy and water absorption bands). Fig. 2 shows the spectra of the target and background endmembers. The spectra of soy-clean, corn-notill, corn-mintill, soy-notill and soy-mintill are chosen as desired targets and the spectra of grass/pasture, grass/trees and woods classes are regarded as background endmembers. The synthetic image has 185 spectral bands.

Having generated the background image, a 10 × 18 matrix consisting of target pixels was implanted in the following manner. Two rows of the target matrix correspond to one target. The first column of this matrix replaced the entire background pixel, i.e., first column contains targets with abundance values of 1.

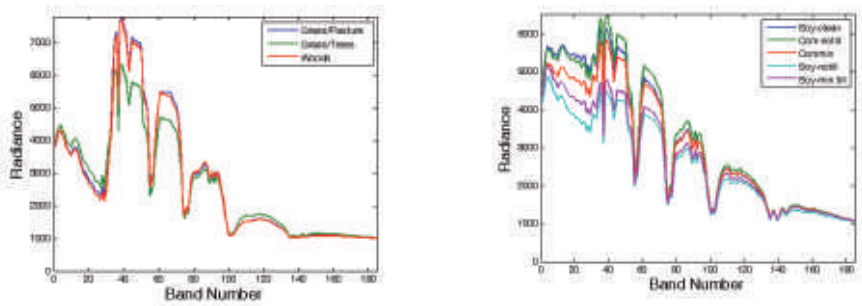

(a) (b)

Fig. 2: Spectral signatures of background and target endmembers, (a) background endmembers and (b) target endmembers.

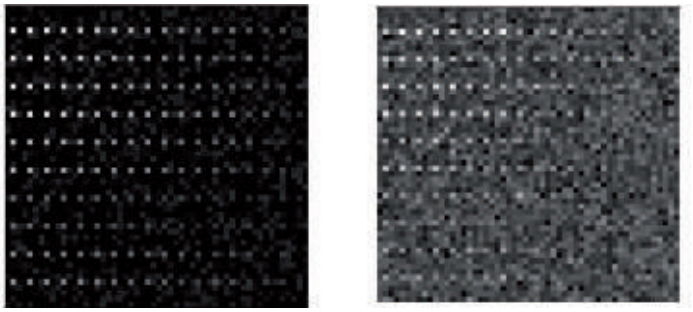

(a) (b)

Fig. 3: Synthetic hyperspectral dataset, (a) 180 simulated target panels and (b) band 30 of the synthetic image with SNR 20:1.

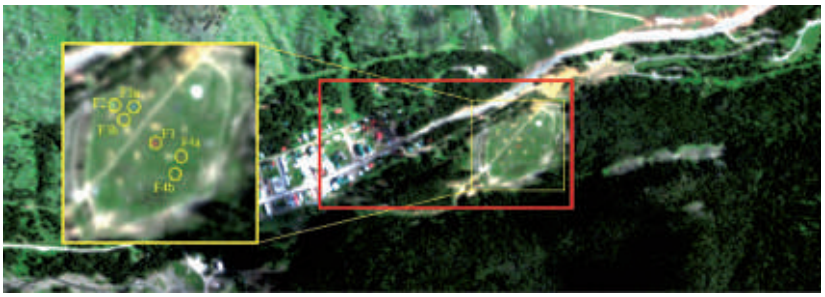

Fig. 4: True colour representation of the HyMap dataset; the red region represents the study area.

In the next column, the abundance values of targets decreased to .95 while the abundance values of background pixels increased to .05. By the same token, this pattern continues till the last column, wherein the abundance values of targets reduce to .15. After generating the synthetic image, it was corrupted by Gaussian additive noise to reach a signal-to-noise ratio (SNR) of 20:1. Fig. 3 shows band 30 of the synthetic image.

Real-world hyperspectral dataset: The second dataset employed in this work is a real hyperspectral reflectance image of size 120×250. This image has been extracted from a larger image acquired by the HyMap airborne hyperspectral sensor over Cook City, MT, U.S., on July 4, 2006. The data have a ground sample distance (GSD) of about 3 m and 126 bands in the VNIR-SWIR range. The scene encompasses several types of land cover classes. During acquisition, several targets with sizes comparable to or smaller than the GSD were placed in open grass fields (Tab. 1) and their reflectances were collected. A true colour image of the scene with highlighted target locations can be seen in Fig. 4 (Snyder et al. 2008).

4.2 *Organization of the Experiment*

The experiment was organized as follows:

Signal subspace identification and endmember extraction: In case of using real-world data, the background endmembers are not known *a priori*. However, some of the aforementioned detectors require this *a priori* knowledge (i.e., background endmembers). So, two key issues have to be addressed. One is the number of endmembers assumed to be present in the hyperspectral data, which is referred to as virtual dimensionality (VD) (Chang & Du 2004). Another is how to estimate these endmembers once the VD is determined. There are some algorithms to estimate these quantities. In this paper, the HySime and VCA were used to estimate the signal subspace dimension and the endmembers' spectra, respectively. Two reasons can justify the use of these two al-

Tab. 1: HyMap target characteristics.

TargetName	Colour	Material	Units	Size
F1	Red	Cotton	1	3m×3m
F2	Yellow	Nylon	1	3m×3m
F3	Blue	Cotton	2	2m×2m, 1m×1m
F4	Red	Nylon	2	2m×2m, 1m×1m

gorithms: 1) the HySime method is unsupervised and fully automatic (i.e., it does not depend on any tuning parameters) (Broadwater & Chellappa 2007), and 2) the VCA achieves state-of-the-art performance with a computational complexity between one and two orders of magnitude lower than the best algorithms (Nascimento & Bioucas-Dias 2005).

As stated in section 2, the ACE and CEM algorithms assume no background signatures, which removes the need to extract and identify the proper number of background endmembers. However, as noted in section 2, the CEM approach has a significant shortcoming. It is very sensitive to the noise. As was shown in (Chang & Heinz 2000), the noise sensitivity is closely related to the number of eigenvectors to be used to calculate $R_{L\times L}^{-1}$ and the intrinsic dimensionality of a hyperspectral image, which is usually less than the data dimensionality L. If the number of eigenvectors (q) is known *a priori* (q, for example), we can use SVD so that $R_{L\times L}$ can be reduced to $\tilde{R}_{L\times L}=\tilde{V}\Lambda\tilde{V}^T$, where $\tilde{V}=(\tilde{v}_1,\tilde{v}_2,...,\tilde{v}_q)$ is an eigenmatrix, $\tilde{v}_k$ is the L-dimensional vector corresponding to the kth eigenvalue λ_k, and $\Lambda=diag\{\lambda_1,\lambda_2,...,\lambda_q\}$ is a diagonal matrix with eigenvalues as diagonal elements. Using this eigen-decomposition, the inverse of $\tilde{R}_{L\times L}=\tilde{V}\Lambda\tilde{V}^T$ can be found by $\tilde{R}_{L\times L}^{-1}=\tilde{V}\Lambda^{-1}\tilde{V}^T$ (Harsanyi 1993). Criteria for choosing the number of basis vectors are mostly based on the percent of variability explained by the first q vectors. Since the SVD is very efficient in capturing the directions (vectors) explaining most of the variability, a relatively small number of basis vectors tends to explain more than 99.99% of the overall variability (Ientilucci 2005). So, we use the SVD to compute the inverse of sample correlation matrix.

Target detection: After endmember extraction, target detection methods will be applied. Before decision fusion the outputs of detectors for each target are made comparable by scaling them to the [0-1] interval.

Decision fusion: By combining the individual outputs, we aim at a higher accuracy than that of the best classifier. There is a consensus among the researchers in classifier combination that the major factor for a better accuracy is the diversity in the classifier team and, so, the fusion method is of a secondary importance (Kuncheva 2002). In other words, diversity among the members of a team of classifiers is deemed to be a key issue in classifier combination (Kuncheva & Whitaker 2003). Thus, we suggest using a GA to design a multiple-classifier system corresponding to each of the fusion rules.

In GA, binary coding scheme is used. The chromosome length is determined based on the number of the detectors. The process starts by generating a population equal to the chromosome length based on Goldberg's rule of thumb (Goldberg 1989). For initialization all chromosome bits are set to one. In other words, GA starts using all detectors. Binary tournament selection is applied for parent selection. Two point crossover is used, where the crossover probability and the mutation rate are set to .8 and .03, respectively. As the stopping condition for the algorithm, the number of generations is set to 50.

Detection performance: For any given target detector or binary classifier, its performance is described via the receiver operating characteristic (ROC) curve, which plots detection rate versus false alarm rate for all possible thresholds (i.e., [1~0]). Generally, the area under the curve (AUC) is used as a metric to evaluate detection performance independent of threshold selection. Since we have more than two targets (or classes) here, the mean detection rate R_D and mean false alarm rate R_F

can be defined by taking the mean of detection rate and false alarm rate over all targets as $\overline{R}_D = \sum_{j=1}^{p} w_j R_{D,j}$ and $\overline{R}_F = \sum_{j=1}^{p} w_j R_{F,j}$, respectively, where $w_j = \frac{N_j}{N_{1,\ldots,p}}$, N_j is the number of j-th target pixels and $N_{1,\ldots,p}$ is the total number of all target pixels (CHANG et al. 2001). Here, GA aims to maximize the AUC, i.e., the AUC is used as the fitness measure.

4.3 *Experimental Results on Synthetic Dataset*

As stated in the previous section, detection performance is described via the AUC. Tab. 2 shows the AUC of target detectors as well as the number of false alarm pixels for the detection probability of .9. It can be induced that in terms of AUC and number of false alarm (FA) pixels, the ACE and CEM algorithms showed the best performance. At first sight, it seems that fusing the results of these detectors with those of others may deteriorate the fusion output; however, fusion results, especially in case of mean and median rules, show the efficiency of the fusion scheme.

Although fusing detection results increases the detection performance, the choice of the detectors to take the results from is also of vital importance. So, in order to choose the most optimum subset of detectors for each fusion rule via GA, the AUC of the first two targets

Tab. 2: AUC and number of false alarm pixels (synthetic dataset).

Detector	Mean AUC	Number of False Alarm Pixels					Mean False Alarm Pixels
		Soy-clean	**Corn-notill**	**Corn-mintill**	**Soy-notill**	**Soy-mint-ill**	
OSP	0.643	1997	2175	2171	2617	2118	2216
CEM	0.968	92	104	344	281	292	223
TCIMF	0.634	2025	2167	2031	2536	2061	2164
ACE	0.958	81	61	200	508	812	332
AMSD	0.556	2880	2880	2880	2880	2880	2880
FCLS	0.875	103	175	2880	2880	2880	1784
NCLS	0.869	211	2880	2880	2880	2880	2346
SCLS	0.688	1703	2146	2192	2776	2059	2175
Max (DS*)	0.968	92	104	344	281	191	223
Mean (DS)	0.976	52	67	211	186	121	127
Median (DS)	0.974	71	51	237	589	85	207
Min (DS)	0.957	80	61	272	413	541	273
Product (DS)	0.954	72	78	153	885	528	343

*detector selection (via GA)

Tab. 3: Optimum detectors for each decision fusion rule (synthetic dataset).

	OSP	CEM	TCIMF	ACE	AMSD	FCLS	NCLS	SCLS
Max	0	1	0	0	0	1	1	0
Mean	0	1	0	0	0	1	0	0
Median	1	1	0	1	0	1	1	1
Min	0	1	0	1	0	0	0	1
Product	0	0	0	1	0	0	0	1

Tab. 4: Effect of optimum detector selection (synthetic dataset).

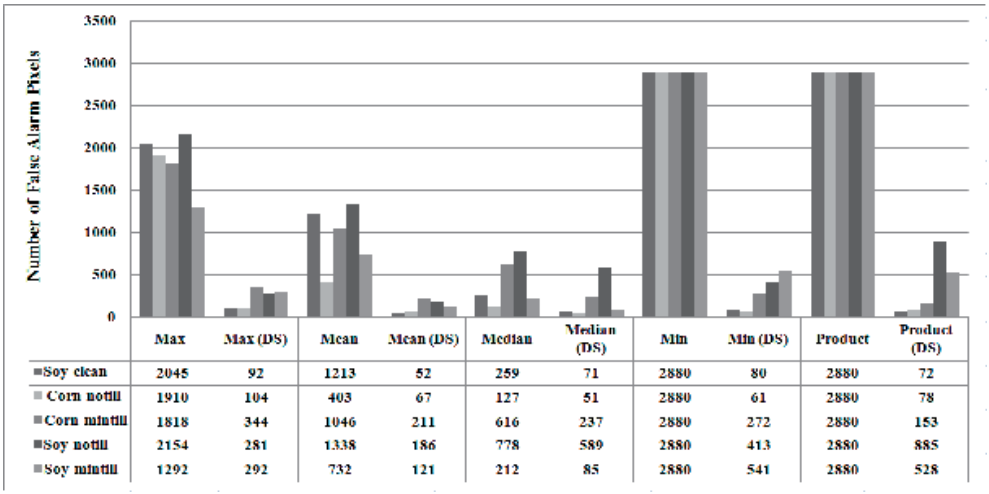

	Max	Max (DS)	Mean	Mean (DS)	Median	Median (DS)	Min	Min (DS)	Product	Product (DS)
Soy clean	2045	92	1213	52	259	71	2880	80	2880	72
Corn notill	1910	104	403	67	127	51	2880	61	2880	78
Corn mintill	1818	344	1046	211	616	237	2880	272	2880	153
Soy notill	2154	281	1338	186	778	589	2880	413	2880	885
Soy mintill	1292	292	732	121	212	85	2880	541	2880	528

(soy-clean and corn-notill) are chosen as the fitness measure. Final chromosomes corresponding to each decision fusion rule are presented in Tab. 3.

It is worth mentioning that the mean rule as the best decision fusion rule does not make use of ACE. Instead it uses the detection outputs of FCLS, which are notably worse than the ACE outputs. Tab. 4 demonstrates the effectiveness of choosing optimum detectors. It can be induced that detector selection strategy causes a dramatic drop in the number of FA pixels in all cases.

4.4 *Experimental Results on Real-World Data*

In the case of the HyMap dataset, a limited number of target pixels would prevent a reliable estimate of the detection probability and leads to a sparse ROC curve. Therefore, the detection performance is evaluated by finding the highest test statistics within the region of interest (ROI) and by counting the number of pixels in the image with a higher value. Hence, the resulting value is the number of false alarms arising from the detection of the given target (Matteoli et al. 2011). Therefore, in this case GA aims at minimizing the number of false alarm pixels instead of maximizing the AUC. Here, the sum of FA pixels of targets 1 and 3 is regarded as GA fitness function. As mentioned before, the HySime and VCA methods are used to estimate the signal subspace and endmembers, respectively. The HySime method is applied to the HyMap subset and the signal subspace dimension of 21 is obtained.

As mentioned, the CEM algorithm is sensitive to noise, and the noise sensitivity is closely related to the number of eigenvectors to be used to calculate $\tilde{R}_{L\times L}^{-1}$, so the number of eigenvectors is chosen such that 99.99% of the data variance is maintained.

Quantitative results on the real-world hyperspectral data, containing the number of FA pixels, are tabulated in Tab. 5. It can be observed that regardless of the physical constraints imposed on the FCLS and NCLS detectors, their detection performance is lower than the SCLS algorithm; however, from the material quantification point of view (i.e., estimating true abundance fraction) this might not be true. In the case of material quantification it is necessary to satisfy nonnegativity and sum-to-one constraints. But in the case of target detection the satisfaction of the aforementioned constraints is not necessary. As mentioned in Chang & Heinz (2000) this unconstrained disadvantage turns out to be an advantage in the detection of targets. It also can be inferred that similar to the previous case, the mean fusion rule outperforms the best detector (i.e., OSP).

The comparative results of conventional fusion rules and the proposed method are pre-

Tab. 5: Number of false alarm pixels (real-world data).

Detector	Number of False Alarm Pixels				Mean False Alarm Pixels
	1st target	**2nd target**	**3rd target**	**4th target**	
OSP	2	0	71	23	24
TCIMF	0	0	1207	0	302
AMSD	5	0	347	280	158
FCLS	145	646	154	29990	7734
NCLS	377	572	342	29990	7820
SCLS	1	0	78	40	30
ACE	0	0	3945	0	986
CEM	126	447	607	285	366
Max (DS)	2	0	82	41	31
Mean (DS)	0	0	64	2	17
Median (DS)	0	0	156	6	41
Min (DS)	14	1	9	29990	7504
Product (DS)	3	0	13	29990	7502

Tab. 6: Effect of optimum detector selection (real-world data).

Fusion rule	Number of False Alarm Pixels				Mean False Alarm Pixels
	1st target	2nd target	3rd target	4th target	
Max	5	3	191	5	51
Max (DS*)	2	0	82	41	31
Mean	0	0	158	4	41
Mean (DS)	0	0	64	2	17
Median	0	0	385	2	97
Median (DS)	0	0	156	6	41
Min	14	1	9	29990	7504
Min (DS)	14	1	9	29990	7504
Product	3	0	13	29990	7502
Product (DS)	3	0	13	29990	7502

*detector selection (via GA)

Tab. 7: Optimum detectors for each decision fusion rule (real-world data).

	OSP	CEM	TCIMF	ACE	AMSD	FCLS	NCLS	SCLS
Max	0	0	0	0	1	0	0	1
Mean	1	1	1	0	0	0	0	1
Median	0	1	1	1	1	1	1	1
Min	1	1	1	1	1	1	1	1
Product	1	1	1	1	1	1	1	1

sented in Tab. 6. The results substantiate the positive impact of detector selection on improving the fusion results. For instance, in the case of the mean rule while taking all detectors into account a mean false alarm rate of 41 is obtained. By selecting the optimum detectors, this number decreases from 41 to 17. However, in the case of min and product rules, detector selection does not affect the final results and all detectors are taken into account. This result is in agreement with what was stated in section 3. In fact, this poor performance is due to wrong assumptions made in these fusion methods.

Comparing the results of the proposed approach with conventional fusion rules in Tabs. 4 and 6 show a drop of the number of false alarm pixels. As stated before, the major factor to obtain a better fusion result is the diversity among classifiers, so it can be implied that the proposed approach fulfills the diversity condition.

Tab. 7 shows the output chromosomes of GA corresponding to each decision fusion rule. It can be seen that just as in the synthetic dataset experiment, the mean rule as the best fusion rule does not necessarily take advantage of all detectors with high performance. It does not take the AMSD results into account, but it chooses the CEM detector instead, which in this case contains higher FA pixels compared to AMSD.

5 Conclusions

In this paper, a decision fusion approach for improving hyperspectral subpixel target detection performance was proposed. To illustrate the efficiency of the proposed method, a synthetic and a real-world hyperspectral dataset were used. Since in conventional fusion rules the redundancy in the detectors' outputs may lead to error propagation, the success of each fusion rule is highly dependent on creating diversity using GA. The proposed method showed that decision fusion is an effective yet simple tool to better detection results. Furthermore, experimental results on both datasets showed that the mean fusion rule is a reliable and robust solution to improve detection perfomance. Although this research showed the success of fusion approach to improve detection performance, due to lack of training data in detection applications, further research on developing unsupervised methods to measure the diversity among detectors' outputs is required.

Acknowledgement

We wish to express our appreciation to Dr. John Kerekes of the Rochester Institute of Technology for providing the HyMap dataset.

References

Alexandre, L., Campilho, A. & Kamel, M., 2001: On combining classifiers using sum and product rules. – Pattern Recognition Letters **22** (12): 1283–1289.

Bioucas-Dias, J. & Nascimento, J., 2008: Hyperspectral Subspace Identification. – IEEE Transactions on Geoscience and Remote Sensing **46** (8): 2435–2445.

Bro, R. & Jong, S., 1997: A fast non-negativity-constrained least squares algorithm. – Journal of Chemometrics **11** (5): 393–401.

Broadwater, J. & Chellappa, J., 2007: Hybrid detectors for subpixel targets. – IEEE Trans. Geoscience Remote Sensing **29** (11): 1891–1903.

Chang, C.I., 2005: Orthogonal Subspace Projection (OSP) Revisited: A Comprehensive Study and Analysis. – IEEE Transactions on Geoscience and Remote Sensing **43** (3): 502–518.

Chang, C.I. & Du, Q., 2004: Estimation of number of spectrally distinct signal sources in hyperspectral imagery. – IEEE Transactions on Geoscience and Remote Sensing **42** (3): 608–619.

Chang, C.I. & Heinz, D., 2000: Constrained Subpixel Target Detection for Remotely Sensed Imagery. – IEEE Transactions on Geoscience and Remote Sensing **38** (3): 1144–1159.

Chang, C.I., Chiang, S.S., Du, Q., Ren, H. & Ifarragaerri, A., 2001: An ROC analysis for subpixel detection. – IEEE 2001 International Geoscience and Remote Sensing Symposium: 2355–2357.

Dasarathy, B., 1994: Decision Fusion. – IEEE Computer Society Press.

Du, Q., Ren, H. & Chang, C.I., 2003: A Comparative Study for Orthogonal Subspace Projection and Constrained Energy Minimization. – IEEE Transactions on Geoscience and Remote Sensing **41** (6): 1525–1529.

Duin, R., 2002: The Combining Classifier: to Train or Not to Train? – Proceedings 16th International Conference on Pattern Recognition **2:** 765–770.

Goldberg, D.E., 1989: Sizing populations for serial and parallel genetic algorithms. – **3rd** International Conference on Genetic Algorithms: 70–79.

Harsanyi, J. & Chang, C.I., 1994: Hyperspectral image classification and dimensionality reduction: An orthogonal subspace projection approach. – IEEE Transactions on Geoscience and Remote Sensing **32** (4): 779–785.

Harsanyi, J.C., 1993: Detection and classification of subpixel spectral signatures in hyperspectral image sequences. – Ph.D. dissertation, Dept. Electrical Eng., Univ. Maryland, Baltimore County.

Heinz, D. & Chang, C.I., 2001: Fully constrained least squares linear spectral mixture analysis method for material quantification in hyperspectral imagery. – IEEE Transactions on Geoscience and Remote Sensing **39** (3): 529–545.

Heinz, D., Chang, C.I. & Althouse, M., 1999: Fully constrained least-squares based linear unmixing. – IEEE 1999 International Geoscience and Remote Sensing Symposium: 1401–1403.

Hsieh, P.F. & Landgrebe, D., 1998: Classification of high dimensional data. – Ph.D. dissertation, School of Electrical and Computer Eng., Purdue Univ., West Lafayette.

Ientilucci, E., 2005: Hyperspectral Sub-Pixel Target Detection Using Hybrid Algorithms and and Physics Based Modeling. – Ph.D. dissertation, Chester F. Carlson Center for Imaging Science, Rochester Institute of Technology, Rochester, New York.

Kraut, S., Scharf, L.L. & Butler, R.W., 2005: The adaptive coherence estimator: A uniformly most-powerful-invariant adaptive detection statistic. – IEEE Transactions on Geoscience and Remote Sensing **53** (2): 427–438.

Kuncheva, L.I., 2002: A Theoretical Study on Six Classifier Fusion Strategies. – IEEE Transactions on Pattern Analysis and Machine Intelligence **24** (2): 281–286.

Kuncheva, L.I. & Whitaker, C., 2003: Measures of Diversity in Classifier Ensembles and Their Relationship with the Ensemble Accuracy. – Machine Learning **51** (2): 181–207.

Mangari, U., Samanta, S., Das, S. & Cho, P., 2010: A Survey of Decision Fusion and Feature Fusion Strategies for Pattern Classification. – IETE Technical Review **27** (4): 293–307.

Manolakis, D. & Shaw, G., 2002: Detection Algorithms for Hyperspectral Imaging Applications. – IEEE Signal Processing Magazine **19** (1): 29–43.

Manolakis, D., Marden, D. & Shaw, G.A., 2003: Hyperspectral image processing for automatic target detection applications. – Lincoln Lab. Journal **14** (1): 79–116.

Manolakis, D., Siracusa, C. & Shaw, G., 2001: Hyperspectral subpixel target detection using the linear mixing model. – IEEE Transactions on Geoscience and Remote Sensing **39** (7): 1392–1409.

Matteoli, S., Ientilucci, E.J. & Kerekes, J.P., 2011: Operational and performance considerations of radiative-transfer modeling in hyperspectral target detection. – IEEE Transactions on Geoscience and Remote Sensing **49** (4): 1343–1355.

Nascimento, J. & Bioucas-Dias, J., 2005: Vertex component analysis: a fast algorithm to unmix hyperspectral data. – IEEE Transactions on Geoscience and Remote Sensing **43** (4): 898–910.

Ren, H. & Chang, C.I., 2000: A target-constrained interference-minimized filter for subpixel detection in hyperspectral imagery. – IEEE 2000 International Geoscience and Remote Sensing Symposium.

Snyder, D., Kerekes, J., Fairweather, I., Crabtree, R., Shive, J. & Hager, S., 2008: Development of a web-based application to evaluate target finding algorithms. – IEEE 2008 International Geoscience and Remote Sensing Symposium: 915–918.

Xu, L., Krzyzak, A. & Suen, C., 1992: Methods of Combining Multiple Classifiers and Their Applicaton to Handwriting Recognition. – IEEE Transactions on Systems, Man and Cybernetics **22** (3): 380–384.

Zhang, L., Du, B. & Zhong, Y., 2010: Hybrid Detectors Based on Selective Endmembers. – IEEE Transactions on Geoscience and Remote Sensing **48** (6): 2633–2646.

Addresses of the Authors:

Hamed Gholizadeh & Mohammad Javad Valadan Zoej, Faculty of Geodesy and Geomatics, K.N. Toosi University of Technology, Tehran, P.O. Box 15875-4416, Iran, Tel: +98-21-88786212, Fax: +98-21-88786213; e-mail: h_gholizade@sina.kntu.ac.ir & valadanzouj@kntu.ac.ir.

Barat Mojaradi, School of Civil Engineering, Iran University of Science and Technology, Tehran, P.O. Box: 16765-163, Iran, Tel: +98-21-77240399, Fax: +98-21-77240398, e-mail: mojaradi@iust.ac.ir.

Manuskript eingereicht: November 2011
Angenommen: Januar 2012